

Quantum Monte Carlo calculations of the one-body density matrix and excitation energies of silicon

P. R. C. Kent, Randolph Q. Hood, M. D. Towler, R. J. Needs, and G. Rajagopal
Cavendish Laboratory, Madingley Road, Cambridge CB3 0HE, United Kingdom.

(Received 8 October 1997)

Quantum Monte Carlo (QMC) techniques are used to calculate the one-body density matrix and excitation energies for the valence electrons of bulk silicon. The one-body density matrix and energies are obtained from a Slater-Jastrow wave function with a determinant of local density approximation (LDA) orbitals. The QMC density matrix evaluated in a basis of LDA orbitals is strongly diagonally dominant. The natural orbitals obtained by diagonalizing the QMC density matrix resemble the LDA orbitals very closely. Replacing the determinant of LDA orbitals in the wave function by a determinant of natural orbitals makes no significant difference to the quality of the wave function's nodal surface, leaving the diffusion Monte Carlo energy unchanged. The Extended Koopmans' Theorem for correlated wave functions is used to calculate excitation energies for silicon, which are in reasonable agreement with the available experimental data. A diagonal approximation to the theorem, evaluated in the basis of LDA orbitals, works quite well for both the quasihole and quasielectron states. We have found that this approximation has an advantageous scaling with system size, allowing more efficient studies of larger systems.

PACS: 71.10.-w, 71.20.-b, 71.55.Cn

I. INTRODUCTION

The two most common, practical quantum Monte Carlo (QMC) methods for realistic systems are the variational quantum Monte Carlo (VMC)^{1,2} and diffusion quantum Monte Carlo (DMC)^{2,3} methods. In VMC, expectation values are computed with an approximate many-body trial wave function. In DMC, imaginary time evolution of the many-body Schrödinger equation in principle gives exact results, although in practice one needs to make the “fixed-node approximation” to account for the antisymmetry of the many-electron wave function. In the fixed node approximation, the nodes of the propagated wave function are restricted to those of the trial wave function. The accuracy of this approximation is central to DMC simulations of many-electron systems. One of the aims of our work is to investigate the effectiveness of this approximation for extended systems, with the long term goal of obtaining better trial wave functions.

In this paper we calculate the one-body density matrix for the valence electrons of silicon within the VMC framework, and obtain the natural orbitals which diagonalize the density matrix. These calculations require the whole of the density matrix throughout all of the six-dimensional space $\mathbf{r} \times \mathbf{r}'$, not just at a few points in space as has been obtained before. To our knowledge this is the first time that the one-body density matrix and natural orbitals have been obtained for an extended, inhomogeneous, interacting electron system. Recent evidence has suggested⁴ that a determinant of natural orbitals may give a better nodal surface than a determinant of Hartree-Fock (HF) orbitals. Our results show that a determinant of natural orbitals has a similar quality nodal surface to a determinant of LDA orbitals for bulk silicon. In a separate calculation we find that a determinant of

LDA orbitals has a slightly better nodal surface than a determinant of HF orbitals.

There is considerable interest in calculating excitation energies using QMC techniques. Excitation energies may be obtained by analyzing DMC decay curves,^{5,6} but this method has not proven very useful due to the large statistical noise. Furthermore, as the quality of the ground state trial wave function improves, less information about excited states is obtained. A combination of ground and excited state wave functions must then be used to obtain upper bounds for the excitation energies. Direct methods for calculating excitation energies have met with more success. Mitáš and Martin have calculated an excitation energy in a molecular nitrogen solid by performing DMC calculations for the ground and excited states.⁷ Mitáš has also reported similar calculations for two excitation energies in diamond.⁸ Recently⁹ we used the same method to calculate 27 excitation energies in silicon, obtaining very good agreement with experiment for the low lying excitation energies, while the energies of the higher lying excitations were somewhat too large. In this paper we calculate excitation energies using a different approach. Here we use the “Extended Koopmans' Theorem” (EKT),^{10,11} which derives from quantum chemistry, and involves the one-body density matrix. We have applied this theorem within VMC to calculate the excitation energies of silicon at four inequivalent \mathbf{k} -points within the Brillouin zone. The energies are in good agreement with the available experimental data with a level of agreement similar to direct excitation calculations. We also test the diagonal approximation to the EKT evaluated using the LDA orbitals, which was used previously to estimate quasihole energies in silicon¹³ and NiO.¹⁴ We find that the approximation performs well in silicon and that it has an advantageous scaling with system size. This allows more

efficient studies of excitations in large systems than are possible with existing direct techniques.

The layout of this paper is as follows. In section II we briefly describe the QMC techniques used in our calculations, including the Hamiltonian, the trial wave function and the relevance of natural orbitals to QMC calculations. In section III we present and discuss our results for the one-body density matrix and the natural orbitals of silicon. In section IV we describe the Extended Koopmans' Theorem and its application to the band structure of silicon.

II. QMC SIMULATIONS OF SILICON

In this section we briefly describe our QMC calculations. For a more detailed discussion of the methods we refer the reader to the literature.^{2,3,15-17}

A. The Hamiltonian

For this study we used an fcc simulation cell, with periodic boundary conditions, containing 54 Si⁴⁺ ions and 216 electrons. The Hamiltonian for our system, within the Born-Oppenheimer approximation, is

$$\hat{H} = \sum_i -\frac{1}{2}\nabla_i^2 + \sum_i \sum_\alpha v_\alpha(\mathbf{r}_i, \mathbf{d}_\alpha) + \frac{1}{2} \sum_i \sum_{j \neq i} v(\mathbf{r}_i, \mathbf{r}_j) + \frac{1}{2} \sum_\alpha \sum_{\beta \neq \alpha} v_{\alpha\beta}(\mathbf{d}_\alpha, \mathbf{d}_\beta) . \quad (1)$$

The positions of the N electrons in the supercell are denoted by \mathbf{r}_i and the ion locations are denoted by \mathbf{d}_α . The electron-ion potential, v_α , is modeled by a norm-conserving non-local pseudopotential¹⁸ obtained from atomic calculations performed within the local density approximation (LDA) to density functional theory. The standard method for including the inter-particle Coulomb interactions in periodic systems is to use the Ewald interaction potential. We have found that this interaction gives rise to significant finite size errors, especially for small simulation cells. Recently we introduced a new formulation of the electron-electron interaction for simulations using periodic boundary conditions which eliminates this problem¹⁷ (hereafter referred to as the ‘‘cutoff interaction’’). This interaction satisfies the conditions that (i) it gives the correct Hartree energy and (ii) it has the proper $1/r$ form for the interaction of an electron with its exchange-correlation hole. (The Ewald interaction violates condition (ii).) Here we present results for excitation energies calculated with both the Ewald and cutoff interactions, using a wave function which was optimized using the cutoff interaction. For consistency one should use the same form of interaction between all the particles, but it turns out that if we apply our new interaction to a system of quantum mechanical electrons

and classical ions then it reduces to using the Ewald interaction for the terms involving the ions while the cutoff interaction applies only to the electron-electron interactions. Note that the cutoff interaction is formulated independently of QMC itself and may be used with other techniques for periodic systems.¹⁷

B. The trial wave function

The choice of trial wave function is of critical importance for VMC and DMC calculations. We have used a standard Slater-Jastrow form:

$$\Psi_T(\mathbf{r}_1, \dots, \mathbf{r}_N) = D^\uparrow(\mathbf{r}_1, \dots, \mathbf{r}_{\frac{N}{2}}) D^\downarrow(\mathbf{r}_{\frac{N}{2}+1}, \dots, \mathbf{r}_N) \times \exp\left(\sum_{i=1}^N \chi(\mathbf{r}_i) - \sum_{i<j}^N u(r_{ij})\right) , \quad (2)$$

where the spin-up and spin-down Slater determinants, D^\uparrow and D^\downarrow , are multiplied by a Jastrow factor which contains a one-body χ function and two-body correlation factor, u . Our χ -function has the full symmetry of the diamond structure and is expressed as a Fourier series containing 6 inequivalent, non-zero, parameters. We used spherically symmetric parallel and antiparallel spin u -functions,¹⁶ which satisfy the electron-electron cusp conditions¹⁹ and contain a total of 16 parameters. The optimized parameter values were obtained by minimizing the variance of the energy.¹⁶

The spin-up and spin-down Slater determinants were formed from single-particle orbitals obtained from an LDA calculation employing the same pseudopotential as in the QMC calculations. The LDA orbitals were calculated at the Γ -point of the simulation cell Brillouin zone using a plane wave basis set with an energy cutoff of 15 Ry. Although the Γ -point scheme does not give optimal Brillouin zone sampling,²⁰ it does preserve the full symmetry of the system and allows comparison with a wider number of established results. The Γ -point of the simulation cell Brillouin zone unfolds to four inequivalent \mathbf{k} -points in the primitive Brillouin zone. These are: (0,0,0) (the Γ -point), $(0,0,\frac{2}{3})\frac{2\pi}{a}$ (a point along the Δ axis, hereafter referred to as the Δ -point), $(0,\frac{2}{3},\frac{2}{3})\frac{2\pi}{a}$ (a point along the Σ axis, hereafter referred to as the Σ -point), and $(\frac{1}{3},\frac{1}{3},\frac{1}{3})\frac{2\pi}{a}$ (a point along the Λ axis, hereafter referred to as the Λ -point).

It is highly desirable to improve the quality of the trial wave functions used in QMC calculations. Improvements to trial wave functions can be classified into three types: (i) improvement of the Jastrow factor, (ii) using a linear combination of determinants, and (iii) improvements in the orbitals forming the determinants. In this paper we will investigate a possible improvement of type (iii), namely the use of natural orbitals. The question of which single-particle orbitals lead to the best approximation to the exact many-body wave function is still open. Furthermore, this choice fixes the nodal surface of the trial wave function and therefore determines the accuracy

of the fixed-node approximation. LDA and HF orbitals have been used successfully in a number of atomic,^{16,21} molecular^{22,23} and solid²⁴ QMC calculations, but so far it has not proved possible to perform a direct optimization of the single-particle orbitals of an extended system. A study of first row atoms and molecules^{25,26} showed that lower energies can be obtained in both VMC and DMC using a trial wave function containing several determinants obtained from a multi-configuration self-consistent field (MCSCF) calculation. However, a similar study for small silicon clusters found that trial wave functions containing a single determinant of natural orbitals computed within an MCSCF scheme gave better DMC results than some multi-determinant wave functions.⁴ This result strongly suggests that the natural orbitals result in improved nodal surfaces, and motivates our calculation of the natural orbitals for bulk silicon.

An expansion of a wave function in Slater determinants of natural orbitals requires a smaller number of terms for a given accuracy than expansions using other orbitals.^{27,28} Calculation of the natural orbitals is, however, costly, and less expensive schemes such as natural pair orbitals^{29,30} have been proposed to improve convergence in quantum chemical calculations. It is not clear that orbitals arising in schemes designed to accelerate convergence of configuration interaction (CI) calculations should give smaller fixed-node errors in DMC calculations than LDA or HF orbitals. However, as mentioned above, there is some evidence to suggest that natural orbitals have this property. Natural orbitals have not frequently been computed within fermion QMC, although VMC and DMC calculations of natural orbitals have been reported for the ground states of the Li, C, and Ne atoms.³¹ No calculations of natural orbitals for realistic extended fermion systems have appeared in the literature to date, although for homogeneous systems the translational symmetry requires the natural orbitals to be plane waves.

Systematic studies of multi-determinant wave functions in QMC are lacking for solids. It seems reasonable to assume that multi-determinant wave functions will have improved nodes, and therefore give a better representation of the exact wave function, but there is little direct evidence to support this. Multi-configurational approaches include correlation effects, but do so relatively inefficiently - large numbers of terms (configurations) are usually required to obtain a significant proportion of the correlation energy. This form of wave function is unattractive for QMC as we require an accurate representation of the wave function which can be rapidly evaluated. Therefore, we obtain the one-body density matrix and hence the natural orbitals from a VMC calculation using a correlated trial wave function, bypassing the need to determine them using a multi-determinantal calculation.

C. VMC and DMC calculations

In VMC we compute the expectation value of the Hamiltonian, \hat{H} , or other operator, with a trial wave function, Ψ_T . This method gives a rigorous upper bound to the exact ground state energy. The Metropolis algorithm is used to generate electron configurations, \mathbf{R} , distributed according to $|\Psi_T(\mathbf{R})|^2$, and the energy calculation is performed by averaging the local energy, $\Psi_T^{-1}\hat{H}\Psi_T$, over this distribution.

In our DMC calculations we use the short-time approximation for the Green's function with a time step of 0.015 a.u., which has been shown to give a small time-step error in silicon.³² Importance sampling is introduced via the trial wave function, Ψ_T . We make the fixed node approximation, restricting the nodes of the DMC solution to be those of the trial wave function. Approximately 15×10^3 statistically independent electron configurations were used and the acceptance/rejection ratio was greater than 99.9%. The computational cost of this method scales with the third power of the system size. Exact fermion techniques, such as the release node QMC and CI methods, have computational requirements increasing exponentially with the system size and are impractical for the system sizes used here.

III. CALCULATION OF THE DENSITY MATRIX AND NATURAL ORBITALS

A. Density matrix

The one-body density matrix³³ for a normalized wave function, ψ , is defined as

$$\rho(\mathbf{r}, \mathbf{r}') = N \int \psi^*(\mathbf{r}, \mathbf{r}_2, \dots, \mathbf{r}_N) \times \psi(\mathbf{r}', \mathbf{r}_2, \dots, \mathbf{r}_N) d\mathbf{r}_2 \dots d\mathbf{r}_N. \quad (3)$$

To facilitate calculation we expand the density matrix in a basis of orbitals, ϕ_i , leading to

$$\rho(\mathbf{r}, \mathbf{r}') = \sum_{i,j} \rho_{ij} \phi_i(\mathbf{r}) \phi_j^*(\mathbf{r}'). \quad (4)$$

We refer to the diagonal elements, ρ_{ii} , as the orbital occupation numbers. For wave functions consisting of a single determinant, such as HF or LDA wave functions, the density matrix is idempotent ($\rho = \rho^2$) and takes the form of a sum over the occupied orbitals, i.e.,

$$\rho(\mathbf{r}, \mathbf{r}') = 2 \sum_{i=1}^{N/2} \phi_i(\mathbf{r}) \phi_i^*(\mathbf{r}'), \quad (5)$$

so that the occupation numbers are 2 (including spin degeneracy) for occupied orbitals and 0 for unoccupied orbitals.

We write the matrix elements of the interacting density matrix, ρ_{ij} , as expectation values over the distribution $|\psi|^2$:

$$\rho_{ij} = N \int \phi_i^*(\mathbf{r}_1) \phi_j(\mathbf{r}') \frac{\psi(\mathbf{r}', \mathbf{r}_2, \dots, \mathbf{r}_N)}{\psi(\mathbf{r}_1, \dots, \mathbf{r}_N)} \times |\psi(\mathbf{r}_1, \dots, \mathbf{r}_N)|^2 d\mathbf{r}' d\mathbf{r}_1 \dots d\mathbf{r}_N. \quad (6)$$

The permutation symmetry allows us to rewrite this in a way which is efficient for Monte Carlo evaluation. Denoting the average over the distribution, $|\psi|^2$, as $\langle \dots \rangle_{|\psi|^2}$, the Monte Carlo expectation value is written as

$$\rho_{ij} = \left\langle \sum_{n=1}^N \int \phi_i^*(\mathbf{r}_n) \phi_j(\mathbf{r}') \frac{\psi(\dots, \mathbf{r}', \dots)}{\psi(\dots, \mathbf{r}_n, \dots)} d\mathbf{r}' \right\rangle_{|\psi|^2}, \quad (7)$$

so that N values are accumulated at each step along the VMC walk. The integral over $d\mathbf{r}'$ is performed by summing over a grid of uniform spacing whose origin is chosen randomly for each electron configuration. The same grid in \mathbf{r}' is used for each term in Eq. 7, which further reduces the computational cost. We tested a series of grid sizes for the \mathbf{r}' integral, using identical configurations for each grid size to obtain a correlated sampling estimate of the difference between the integrals. We found that a grid containing 125 points in the simulation cell sampled the integral with sufficient accuracy.

Provided that the density of points in the \mathbf{r}' integral is kept constant, the statistical error in the individual elements of the density matrix for a given number of statistically independent configurations is approximately independent of system size.

We used a basis set consisting of the lowest energy LDA orbitals at the 27 \mathbf{k} -points in the primitive Brillouin zone. We tested the effect of varying the number of orbitals in the basis. We found that approximately 40 orbitals per \mathbf{k} -point were sufficient, although to retain the symmetry we included all members of a degeneracy, so that the actual number used was either 39 or 40 orbitals, depending on the \mathbf{k} -point. The normalization used in Eq. (3) requires that

$$N = \text{Tr}\rho, \quad (8)$$

which provides a practical test for the completeness of the basis set. The total occupation of the matrix ($\text{Tr}\rho$) was 215.9(2), which is within the statistical error of the number of electrons in the system, indicating completeness of the basis at the level of the statistical accuracy obtained.

For a given number of Monte Carlo moves, the best statistics are obtained by accumulating all non-zero matrix elements and applying the symmetry afterwards. However it is computationally very expensive to accumulate all of them, and we found that a more efficient procedure was to accumulate only the independent non-zero matrix elements. The basis set of LDA orbitals are

basis functions of the unitary irreducible representations of the symmetry group O_h^7 . Using the ‘‘orthogonality condition for matrix representations’’³⁴ we inferred that elements involving products of orbitals from inequivalent \mathbf{k} -points and of differing representations are zero. We ensured that every occurrence of a given representation was identical, so that products between functions belonging to different rows were orthogonal. This procedure reduced the total number of independent and non-zero matrix elements, ρ_{ij} , from 42094 to 582 elements.

These matrix elements were sampled using approximately 6.6×10^5 statistically independent configurations. The correlation lengths along the VMC walks of both the local energy and density matrix were found to be essentially the same.

B. Results for the density matrix

We found the matrix ρ_{ij} to be very nearly diagonal, with little coupling between LDA orbitals. Double occupancy (spin-up and down) of orbitals is denoted by the value 2.0. The maximum difference between the interacting occupation number, ρ_{ii} , and the LDA occupation number was 0.0625(5), which occurred at the $\Gamma_{25'}$ state at the top of the valence band. The magnitude of the largest off-diagonal matrix element was 0.014(1), which is of similar order to the occupation number of the lowest unoccupied orbitals. The fractional errors in occupation numbers for orbitals of low occupation were large in comparison to those of high occupation. We found that 97.6% of the total occupation of the density matrix is contained within the four occupied LDA bands at each \mathbf{k} -point, and 99.0% is obtained within the first ten bands. In Fig. 1 we plot the occupation numbers against the LDA band energies. The occupation numbers decrease almost linearly with increasing LDA energy for both the occupied and unoccupied bands.

In Fig. 2 we show the density matrix, $\rho(\mathbf{r}, \mathbf{r}')$, in the (110) plane, and the differences between the VMC and LDA matrices. The coordinate \mathbf{r} is fixed at the center of a covalent bond, and \mathbf{r}' ranges over the (110) plane passing through the atomic positions. The density matrix consists of an asymmetric central peak, reduced in width along the bonding direction. A longer ranged structure is present in areas of high valence charge density, smaller by approximately one order of magnitude than the peak.

The VMC value for the peak in the density matrix on the bond center at $\mathbf{r} = \mathbf{r}'$ is 1.7% smaller than the LDA value. The VMC density matrix has a larger magnitude around the neighboring silicon ions than the LDA density matrix, which consequently has a slightly smaller range. We also examined the density matrix in interstitial regions, where we found more structure to be present. Again, the LDA and VMC results were very similar, with small differences between the two cases arising principally from the differing charge densities.

To investigate the effect of using a finite size simulation cell we compared the LDA density matrix computed for $3 \times 3 \times 3$ and $4 \times 4 \times 4$ \mathbf{k} -point meshes, corresponding to simulation cells containing 54 and 128 atoms respectively. We found that the central peak was largely unchanged and the longer ranged structure was in qualitative agreement. The central maximum in the density matrix in Fig. 2 is at the point $\mathbf{r} = \mathbf{r}'$ and its magnitude is directly proportional to the valence charge density at that point, which differed by 4.9% between the two simulation cell sizes. We expect the finite size effects in the QMC calculations broadly to follow those in the LDA, as we have found for the total energies.¹⁷

In exact Kohn-Sham density functional theory the total energy can be written entirely in terms of the one-body density matrix of the Kohn-Sham orbitals, whereas in a fully interacting system both the one-body density matrix and the pair-correlation function are required. Results for the pair-correlation function from accurate correlated wave functions and LDA calculations are extremely different.³⁵ Exact Kohn-Sham density functional theory reproduces the exact charge density and therefore exactly reproduces the diagonal $\mathbf{r} = \mathbf{r}'$ part of the density matrix. The off-diagonal part of the exact Kohn-Sham and interacting density matrices are not required to be the same. In silicon we expect the LDA to give a good approximation to the exact Kohn-Sham density matrix. For this system our results show that the *entire* density matrices are very similar in VMC and LDA.

C. Natural Orbitals

The natural orbitals were obtained by diagonalizing the density matrix in the basis of the LDA orbitals. An assessment of the statistical errors in the eigenvalues and eigenvectors was made by subjecting the matrix to random perturbations of order the statistical error. The eigenvalues varied by up to ± 0.0004 on application of the small perturbations. All the calculated eigenvalues, λ_i , of the density matrix lie in the range $0 \leq \lambda_i \leq 2$, as is required.³³ Identical results were obtained when elements within statistical error of zero were explicitly zeroed. The overlap of the space occupied by the LDA orbitals and the corresponding natural orbitals is measured by the absolute value of the determinant of the matrix of overlaps between these two sets of vectors. This gave a value of 0.9948, indicating that the spaces spanned are almost the same.

The eigenvalues of the density matrix for the “occupied” natural orbitals were very slightly larger than the corresponding matrix elements ρ_{ii} (by about 0.001). Consequently, the eigenvalues of the “unoccupied” natural orbitals were very slightly decreased, so that $\text{Tr} \rho$ is invariant. Therefore a plot of the eigenvalues of the density matrix would be indistinguishable from Fig. 1, which shows the diagonal elements of the density matrix in the

basis of LDA orbitals.

D. DMC Calculations

As well as the LDA and VMC calculations, we performed fixed node DMC calculations with trial wave functions of the form of Eq. (2), using LDA and natural orbitals to form the determinants. Re-optimization of the Jastrow and χ functions to improve sampling efficiency in the DMC calculation was found to be unnecessary. The resulting energies were -107.59 eV (LDA), $-107.69(1)$ eV (VMC with LDA orbitals), $-107.71(1)$ eV (VMC with natural orbitals), $-108.10(1)$ eV (DMC with LDA orbitals), and $-108.09(1)$ eV (DMC with natural orbitals). The VMC wave function appears to show a very slight improvement with natural orbitals compared with LDA orbitals. However, to within statistical accuracy, the DMC energies obtained with LDA and natural orbitals are the same. This indicates that the nodal surfaces given by the LDA and natural orbitals are of the same quality.

E. DMC Comparison of LDA and HF Orbitals

In light of these results it is interesting to compare the quality of the nodal surfaces obtained with LDA and HF orbitals, which are both commonly used in the determinantal parts of trial wave functions for QMC calculations.

We investigated this by performing DMC calculations in silicon with an fcc simulation cell containing 16 atoms. The smaller simulation cell enabled a large number of independent configurations to be obtained rapidly. Wave functions expanded in a basis of atom-centered Gaussians were obtained from the HF and DFT code³⁶ CRYSTAL95. We took special care to ensure that the LDA and HF calculations were done in equivalent ways to try and eliminate any bias in the comparison. A basis set of four uncontracted *sp* functions and one *d* polarization function per pseudo-atom was optimized separately for each calculation. The quality of the basis set is high - to obtain the same energy within a plane wave calculation would require a basis set cutoff of 12.5 Ry. We used the same non-local LDA pseudopotential as in our other calculations. In both calculations we used the same *u* and χ functions and performed DMC simulations with an average population of 640 walkers, performing approximately 6.7×10^5 walker moves. We obtained DMC total energies of $-107.488(3)$ eV per atom and $-107.464(3)$ eV per atom for the LDA and HF guiding wave functions respectively, using the Ewald interaction in the many-body Hamiltonian.

The walker energies were approximately normally distributed. Using a conventional t-test, the 95% confidence interval on the difference in energies obtained was $0.002 - 0.046$ eV per atom, showing that for this system

it is very likely that the DMC energy from a determinant of LDA orbitals is lower than that from a determinant of HF orbitals. Therefore, for this system, a determinant of LDA orbitals has a marginally better nodal structure than a determinant of HF orbitals.

IV. EXCITATION ENERGIES

A. Excited State Calculations

The calculation of excited state energies in solids using QMC methods is a fairly new area of research. Significant successes have been achieved using direct methods, in which separate QMC calculations are performed for the ground and excited states, and the excitation energy is calculated as the energy difference.⁷⁻⁹ In these direct methods a QMC calculation must be performed for each excitation. In contrast, for the method described here a large number of excitation energies are obtained from a single QMC calculation involving averages over the ground state wave function.

B. The Extended Koopmans' Theorem

Our method for determining excitation energies corresponds to a QMC formulation of the Extended Koopmans' Theorem (EKT) derived independently by Smith, Day and Garrod¹⁰ and by Morrell, Parr and Levy.¹¹ The EKT is closely related to the earlier work of Feynman³⁷ on calculating excitation energies in the superfluid state of He⁴, although the quantum chemists appear to have developed the theory independently. The EKT has been shown to give very good excitation energies for simple molecular systems,³⁸ and has been applied to atomic and diatomic systems.^{39,40} It appears particularly well suited to QMC calculations in which explicitly correlated many-body wave functions are used. Here we review the derivation following Ref. 10 and present our QMC formulation.

1. Valence Band Energies

In this method the band energies are calculated as ionization energies. We start with an approximation to the normalized ground state wave function, ψ^N . The wave function for the $N-1$ electron system is approximated by the Ansatz of eliminating an orbital from ψ^N :

$$\psi^{N-1}(\mathbf{r}_2, \dots, \mathbf{r}_N) = \int u_v^*(\mathbf{r}_1) \psi^N(\mathbf{r}_1, \dots, \mathbf{r}_N) d\mathbf{r}_1. \quad (9)$$

The valence orbital to be eliminated, u_v , will be determined variationally. This Ansatz is reminiscent of a quasiparticle wave function for the excited state, although the formulation is for $N-1$ particle eigenstates of

the Hamiltonian. Expressing Eq. (9) in second quantization yields

$$|\psi^{N-1}\rangle = \hat{O}_v |\psi^N\rangle, \quad (10)$$

where \hat{O}_v is the destruction operator for the state u_v .

The ionization energy is given by the difference in the expectation values of the Hamiltonian calculated with the N and $N-1$ electron wave functions:^{11,41}

$$\epsilon_v = \langle \psi^N | \hat{H} | \psi^N \rangle - \frac{\langle \hat{O}_v \psi^N | \hat{H} | \hat{O}_v \psi^N \rangle}{\langle \hat{O}_v \psi^N | \hat{O}_v \psi^N \rangle}. \quad (11)$$

If ψ^N is an eigenfunction of \hat{H} , Eq. (11) may be written as

$$\epsilon_v = - \frac{\langle \psi^N | \hat{O}_v^\dagger [\hat{H}, \hat{O}_v] | \psi^N \rangle}{\langle \psi^N | \hat{O}_v^\dagger \hat{O}_v | \psi^N \rangle}. \quad (12)$$

The denominator in Eq. (12) is the one-body density matrix. We now expand in a set of orbitals, $\{\phi_i\}$, so that $u_v(\mathbf{r}) = \sum c_{iv} \phi_i(\mathbf{r})$, and $\hat{O}_v = \sum c_{iv} \hat{a}_i$, where \hat{a}_i is the destruction operator for ϕ_i . The condition for a stationary value of ϵ_v generates a secular equation

$$(\mathbf{V}^v - \epsilon_v \mathbf{S}^v) \mathbf{c}_v = \mathbf{0}. \quad (13)$$

The matrix \mathbf{S}^v is the one-body density matrix, and the elements of \mathbf{V}^v are $V_{ij}^v = \langle \psi^N | \hat{a}_j^\dagger [\hat{H}, \hat{a}_i] | \psi^N \rangle$, where

$$V_{ij}^v = N \int \phi_i(\mathbf{r}_1) \phi_j^*(\mathbf{r}') \psi^*(\mathbf{r}_1, \dots, \mathbf{r}_N) \times \hat{H}_1 \psi(\mathbf{r}', \mathbf{r}_2, \dots, \mathbf{r}_N) d\mathbf{r}' d\mathbf{r}_1 \dots d\mathbf{r}_N. \quad (14)$$

\hat{H}_1 consists of the terms in the N -electron Hamiltonian of Eq. (1) involving coordinate \mathbf{r}_1 , so that

$$\hat{H}_1 = \hat{h}_1 + \sum_{j \neq 1}^N v(\mathbf{r}_1, \mathbf{r}_j), \quad (15)$$

where \hat{h} consists of the one-body kinetic energy operator and ionic potential, including both local and non-local pseudopotential components, and v is the electron-electron interaction potential.

If a HF wave function is used for ψ^N and the density matrix is expanded in a basis set of HF orbitals, then V_{ij}^v reduces to a matrix with the HF N -particle eigenvalues on the occupied part of the diagonal, and zeros everywhere else. The resulting excitation energies are those given by the well-known Koopmans' theorem.¹² The contents of the EKT method are now reasonably clear. The method consists of a quasiparticle-like Ansatz for the wave function of the $N-1$ particle system, which is used to calculate the ionization energies of the system. Electron correlations are included, but no allowance is made for relaxation of the other orbitals in the presence of the excitation. Although this relaxation can be important in small systems, it is expected to be much less important for excitations in extended systems such as the silicon crystal studied here.

2. Conduction Band Energies

An analogous theory exists for the conduction band energies. The wave function for the $N+1$ electron system is approximated by the Ansatz of adding an orbital to ψ^N :

$$\psi^{N+1}(\mathbf{r}_0, \dots, \mathbf{r}_N) = \hat{A}u_c(\mathbf{r}_0)\psi^N(\mathbf{r}_1, \dots, \mathbf{r}_N), \quad (16)$$

where \hat{A} is the antisymmetrizer and the orbital u_c is to be determined variationally. In second quantization we have

$$|\psi^{N+1}\rangle = \hat{O}_c^\dagger |\psi^N\rangle. \quad (17)$$

The excitation energies ϵ_c are defined by

$$\epsilon_c = \frac{\langle \psi^N | \hat{O}_c [\hat{H}, \hat{O}_c^\dagger] | \psi^N \rangle}{\langle \psi^N | \hat{O}_c \hat{O}_c^\dagger | \psi^N \rangle}. \quad (18)$$

Expanding in a set of orbitals gives $u_c(\mathbf{r}) = \sum c_{ic} \phi_i(\mathbf{r})$ and $\hat{O}_c^\dagger = \sum c_{ic} \hat{a}_i^\dagger$. The coefficients c_{ic} are the solutions of the secular equation

$$(\mathbf{V}^c - \epsilon_c \mathbf{S}^c) \mathbf{c}_c = \mathbf{0}, \quad (19)$$

where the matrix elements are $V_{ij}^c = \langle \psi^N | \hat{a}_i [\hat{H}, \hat{a}_j^\dagger] | \psi^N \rangle$ and $S_{ij}^c = \langle \psi^N | \hat{a}_i \hat{a}_j^\dagger | \psi^N \rangle = \delta_{ij} - \rho_{ij}$.

It is instructive to introduce a new potential with matrix elements $V_{ij} = V_{ij}^v + V_{ij}^c$:

$$\begin{aligned} V_{ij} &= \int \phi_i(\mathbf{r}_0) \hat{h}_0 \phi_j^*(\mathbf{r}_0) d\mathbf{r}_0 \\ &+ N \int \phi_i(\mathbf{r}_0) \phi_j^*(\mathbf{r}_0) v(\mathbf{r}_0, \mathbf{r}_1) \\ &\quad \times |\psi(\mathbf{r}_1, \dots, \mathbf{r}_N)|^2 d\mathbf{r}_0 d\mathbf{r}_1 \dots d\mathbf{r}_N \\ &- N \int \phi_i(\mathbf{r}_0) \phi_j^*(\mathbf{r}_1) v(\mathbf{r}_0, \mathbf{r}_1) \psi(\mathbf{r}_0, \mathbf{r}_2, \dots, \mathbf{r}_N) \\ &\quad \times \psi^*(\mathbf{r}_1, \dots, \mathbf{r}_N) d\mathbf{r}_0 d\mathbf{r}_1 \dots d\mathbf{r}_N. \end{aligned} \quad (20)$$

If we use a HF wave function and expand in a basis of HF orbitals, V_{ij} reduces to a matrix with the HF N -particle eigenvalues on the diagonal, and zeros everywhere else. In this case one can readily identify the second and third terms in Eq. (20) as, respectively, the Hartree and exchange terms. (Similarly V_{ij}^c reduces to the HF energy eigenvalues on the unoccupied part of the diagonal.)

3. VMC formulation of the EKT

We accumulate the matrix elements of V_{ij}^v and V_{ij} , subsequently forming the matrix $V_{ij}^c = V_{ij} - V_{ij}^v$. The matrix elements, V_{ij}^v , are given by

$$\begin{aligned} V_{ij}^v &= N \int \phi_i(\mathbf{r}_1) \phi_j^*(\mathbf{r}') \frac{\hat{H}_1 \psi(\mathbf{r}_1, \dots, \mathbf{r}_N)}{\psi(\mathbf{r}_1, \dots, \mathbf{r}_N)} \\ &\quad \times \frac{\psi(\mathbf{r}', \mathbf{r}_2, \dots, \mathbf{r}_N)}{\psi(\mathbf{r}_1, \dots, \mathbf{r}_N)} |\psi(\mathbf{r}_1, \dots, \mathbf{r}_N)|^2 d\mathbf{r}' d\mathbf{r}_1 \dots d\mathbf{r}_N. \end{aligned} \quad (21)$$

As before, we use the permutation symmetry to write this as

$$\begin{aligned} V_{ij}^v &= \left\langle \sum_{n=1}^N \int \phi_i^*(\mathbf{r}_n) \phi_j(\mathbf{r}') \frac{\hat{H}_n \psi(\mathbf{r}_1, \dots, \mathbf{r}_N)}{\psi(\mathbf{r}_1, \dots, \mathbf{r}_N)} \right. \\ &\quad \left. \times \frac{\psi(\dots, \mathbf{r}', \dots)}{\psi(\dots, \mathbf{r}_n, \dots)} d\mathbf{r}' \right\rangle_{|\psi|^2}, \end{aligned} \quad (22)$$

so that N values are accumulated at each step. The terms contributing to $\hat{H}_n \psi / \psi$ are already available in a VMC calculation, allowing V_{ij}^v to be accumulated with virtually no additional cost beyond that required for the density matrix. An analogous VMC formulation for calculating V_{ij} was used. The single particle terms, \hat{h}_0 , appearing in the first term in Eq. (20) are evaluated directly without using Monte Carlo integration. We found that using Monte Carlo integration for all the terms resulted in a small increase in the variance of the matrix elements. Therefore we prefer to calculate the \hat{h}_0 terms directly. The matrix elements V_{ij}^v and V_{ij} were accumulated at the same time as the elements ρ_{ij} . The full crystal symmetry was again used, which reduces the number of matrix elements which must be accumulated and ensures the correct symmetry in the presence of statistical noise.

C. Results for excitation energies

1. Full EKT results

The correlation lengths along the VMC walks for V_{ij}^v and V_{ij} were found to be similar to those of the local energy and density matrix, and the distribution of statistical errors was similar to that for the density matrix. The elements of V_{ij}^v and V_{ij}^c with the largest statistical errors were the diagonal elements. The statistical error bars on these elements are estimated to be ± 0.2 eV.

The matrix Eqs. 13 and 19 were diagonalized using a generalized eigenvalue solver. The ratios of the statistical error bars to the mean values were significantly larger for the diagonal elements of V_{ij}^v and V_{ij}^c than for ρ_{ij} . Just as for the density matrix, small perturbations were applied to estimate the statistical errors in the eigenvalues and eigenvectors. The numerical stability of the diagonalization was improved by explicitly zeroing elements of V_{ij}^v and V_{ij}^c within statistical error of zero. The accuracy of the eigenvalues was further verified by gradually increasing the number of bands in the diagonalization procedure. The valence and low lying conduction band energies were stable to within ± 0.4 eV.

The resulting band energies are given in Table I and in Fig. 3, with the energy at the top of the valence band set to zero. Of the \mathbf{k} -points computed here, the available experimental data (Exp) is limited to the Γ -point. Because of this we also give empirical pseudopotential (Emp) data⁴³ in Table I and in Fig. 3, which should provide a good interpolation between this data. Results for

the Ewald and cutoff interactions are in good agreement, indicating that the finite size errors are not significant at the level of statistical accuracy obtained here. The energies are in good qualitative agreement with the empirical data at all \mathbf{k} -points except for the upper Σ_1 valence band state, and the Δ_2' conduction band state. The source of the error is principally the value of the diagonal matrix elements for these states, V_{ii}^v and V_{ii}^c (see next section).

The EKT band energies at the Γ -point are in good agreement with the available experimental data, and are also in good agreement with the DMC data from direct calculations of the excitation energies.⁹ The EKT valence band width of 12.9(6) eV is smaller than the value of 13.6(3) eV obtained from the DMC calculations and is in good agreement with the experimental value of 12.5(6) eV. In comparison the HF data shows the well known overestimation of band gaps and band widths which is due to the neglect of correlation energy, the LDA gives excellent valence band energies while the conduction bands are too low in energy by 0.7-1.0 eV, and the *GW* data is in very good agreement with experiment.

The EKT is a formulation for the eigenstates of the $N-1$ and $N+1$ electron systems, while the direct method is aimed at calculating the eigenstates of the N electron system. The EKT and direct results should therefore differ by the exciton binding energy, but this energy is small for silicon and cannot be resolved at the level of statistical accuracy obtained. Depending on the application one would like to be able to choose whether to include excitonic effects, so that it is advantageous to have the different QMC techniques available. Clearly further refinement of excited state QMC methods is required, but the results from the EKT and direct approaches are promising for the study of more strongly correlated systems, for which the LDA and *GW* methods are less reliable.

2. Diagonal approximations

If we neglect the off-diagonal element of V_{ij}^v , V_{ij}^c , and ρ_{ij} then the valence and conduction band energies can be approximated by

$$\epsilon_{iv}^{\text{DEKT}} = \frac{V_{ii}^v}{\rho_{ii}}, \quad \epsilon_{ic}^{\text{DEKT}} = \frac{V_{ii}^c}{1 - \rho_{ii}}, \quad (23)$$

where the superscript DEKT denotes the diagonal approximation to the EKT. This approximation has been used within VMC by Fahy et al.¹³ to calculate quasihole energies in silicon and by Tanaka¹⁴ to calculate quasihole energies in NiO. This approximation has the computational advantage that far fewer matrix elements are required, and also that the problems of statistical noise are reduced, because the values of only two matrix elements enter the calculation of each band energy. However the results are basis set dependent, and could differ significantly between, for example, a HF and LDA basis.

If we use a HF wave function and expand in a basis set of HF orbitals then the matrices V_{ij}^v , V_{ij}^c , and ρ_{ij} are all diagonal, and consequently the full EKT and the DEKT are equivalent. In general, for correlated wave functions, the DEKT gives neither an upper nor lower bound to the energy obtained from the full EKT. Comparison with the data from the DEKT is also made in Table I. The DEKT values are close to the full EKT values, including the two cases mentioned above where the agreement with experiment is poor. The DEKT works quite well for the valence bands and slightly less well for the conduction bands, because the off-diagonal matrix elements of V_{ij}^c coupling the unoccupied states are more significant. In similar VMC calculations for silicon using the DEKT and a simulation cell containing 64 electrons, Fahy et al.¹³ calculated a valence band width of 14.5(4) eV, which is larger than both our value of 13.3(2) eV and the experimental value of 12.5(6) eV. Fahy et al.¹³ also obtained occupation numbers of 1.96(4) and 1.92(3) for the Γ_1 and $\Gamma_{25'}$ valence band states, respectively, which are within error bars of our results of 1.9817(2) and 1.9375(5).

The scaling with system size of the diagonal approximation is very advantageous compared with direct evaluation of excitation energies. In direct methods, the fractional energy change due to the promotion of an electron is considered. This energy change is inversely proportional to the number of electrons in the system, i.e., a ' $\frac{1}{N}$ ' effect. The precision of the calculation must therefore be sufficient to resolve the energy change amid the statistical noise. This requirement is very challenging for small band gap materials, as the system must also be sufficiently large to approximate the infinite solid. In the DEKT, the band energies are computed directly as averages over the square of the ground state wave function, rather than as the difference between averages over the squares of the ground and excited state wave functions. This greatly improves the sampling statistics. We have found that the errors in V_{ii}^v , V_{ii}^c and ρ_{ii} scale as the inverse of the square root of the number of independent electron configurations, independently of the system size. For sufficiently large systems, it therefore requires fewer statistically independent samples in the DEKT to obtain excitation energies to a given statistical accuracy than with direct methods. The scaling behavior of the full EKT is more difficult to analyze because we are required to diagonalize noisy matrix equations, where the number of off-diagonal matrix elements increases as the square of the system size, and where there are certainly statistical correlations between matrix elements.

V. CONCLUSIONS

We have calculated the one-body density matrix for the valence electrons of bulk silicon using QMC techniques.

In real space, the VMC and LDA density matrices are very similar, the greatest differences being due to the

differing charge densities in each case. The natural orbitals, obtained by diagonalizing the density matrix, very closely resemble the LDA orbitals. The occupation numbers of the natural orbitals differ significantly from the non-interacting values, reducing linearly with increasing energy for the LDA occupied bands. The occupations are about 3% lower than the non-interacting value near the top of the valence band, and above the Fermi level, the occupation numbers fall slowly to zero.

A DMC calculation for the ground state energy of silicon using a trial wave function containing a determinant of natural orbitals gives an energy which is almost identical to that obtained using a determinant of LDA orbitals. This shows that the quality of the nodal surfaces is almost identical in each case. We used DMC calculations to compare the quality of the nodal surfaces obtained with LDA and HF orbitals, finding that the LDA orbitals gave a slightly lower DMC energy, indicating that for the system studied the nodal surface of a determinant of LDA orbitals is slightly better. We note that a previous DMC study of small silicon clusters⁴ found that natural orbitals obtained from a multi-configurational Hartree-Fock calculation gave a better nodal surface than a single determinant of HF orbitals.

We have calculated excitation energies in silicon using an extension of Koopmans' theorem applicable to correlated wave functions. The Monte Carlo formulation is very similar to that required to obtain the density matrix. The resulting band energies are in good agreement with the available experimental data.

The success of the VMC-EKT relies on a cancellation of errors between the ground and excited state energies. The wave functions for the excited states contain the variational freedom of the orbitals u_v and u_c . This variational freedom in the orbitals reduces the energy of the $N-1$ and $N+1$ electron states and improves the agreement with experiment. In the diagonal approximation to the EKT (DEKT), the u_v and u_c orbitals are fixed and there is no variational freedom in the excited state wave functions. We have found that the DEKT works quite well for silicon using LDA orbitals for u_v and u_c . The diagonal approximation is exact within HF theory, so that we expect it to be a good approximation for weakly correlated systems.

Greater accuracy could be obtained with more accurate trial functions, or using DMC in the calculation of V_{ij}^v , V_{ij}^c , and ρ_{ij} . In comparison with direct methods of calculating excitation energies,⁷⁻⁹ the EKT has the advantage that only a single calculation involving the ground state is required to obtain many excitation energies.

The EKT involves assumptions about the nature of the excited state wave functions, but nevertheless is a practical method for calculating excitation energies including correlation effects for relatively weakly correlated systems. The diagonal approximation to the EKT has a very advantageous scaling with system size compared

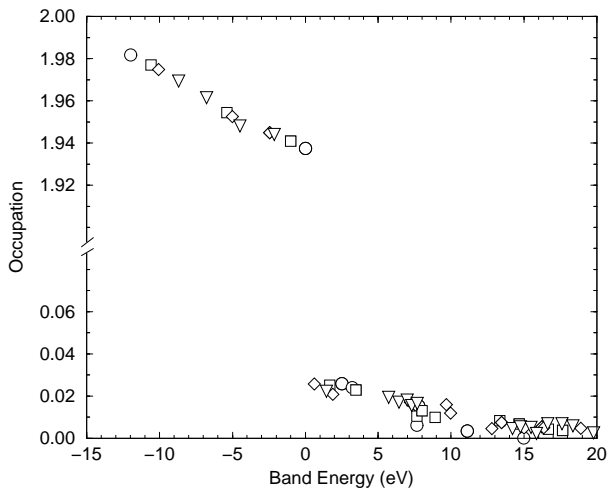
with direct QMC calculations. This scaling thereby allows the study of excitation energies in larger systems with a greater efficiency than is possible with direct techniques.

This work was supported by the Engineering and Physical Sciences Research Council (UK). Our calculations are performed on the CRAY-T3D at the Edinburgh Parallel Computing Centre, and the Hitachi SR2201 located at the University of Cambridge High Performance Computing Facility.

-
- ¹ W. L. McMillan, Phys. Rev. **138**, A442 (1965).
 - ² B. L. Hammond, W. A. Lester, and P. J. Reynolds, *Monte Carlo Methods in Ab Initio Quantum Chemistry* (World Scientific, Singapore, 1994).
 - ³ D. Ceperley, G. Chester, and M. Kalos, Phys. Rev. B **16**, 3081 (1977).
 - ⁴ J. C. Grossman and L. Mitáš, Phys. Rev. Lett. **74**, 1323 (1995).
 - ⁵ M. Caffarel and D. Ceperley, J. Chem. Phys. **97**, 8415 (1992).
 - ⁶ D. M. Ceperley and B. Bernu, J. Chem. Phys. **89**, 6316 (1988).
 - ⁷ L. Mitáš and R. M. Martin, Phys. Rev. Lett. **72**, 2438 (1994).
 - ⁸ L. Mitáš, Comput. Phys. Commun. **96**, 107 (1996).
 - ⁹ A. J. Williamson, R. Q. Hood, R. J. Needs, and G. Rajagopal, unpublished.
 - ¹⁰ O. W. Day, D. W. Smith, and C. Garrod, Int. J. Quantum Chem. Symp. **8**, 501 (1974).
 - ¹¹ M. M. Morrell, R. G. Parr, and M. Levy, J. Chem. Phys. **62**, 549 (1975).
 - ¹² T. Koopmans, Physica **1**, 104 (1924).
 - ¹³ S. Fahy, X. W. Wang, and S. G. Louie, Phys. Rev. Lett. **65**, 1478 (1990).
 - ¹⁴ S. Tanaka, J. Phys. Soc. Japan **64**, 4270 (1995).
 - ¹⁵ S. Fahy, X. W. Wang, and S. G. Louie, Phys. Rev. B **42**, 3503 (1990).
 - ¹⁶ A. J. Williamson, S. D. Kenny, G. Rajagopal, A. J. James, R. J. Needs, L. M. Fraser, W. M. C. Foulkes, and P. Maccallum, Phys. Rev. B **53**, 9640 (1996).
 - ¹⁷ A. Williamson, G. Rajagopal, R. J. Needs, L. Fraser, W. M. C. Foulkes, Y. Wang, and M. Y. Chou, Phys. Rev. B **55**, R4851 (1997).
 - ¹⁸ G. P. Kerker, J. Phys. C **13**, L189 (1980).
 - ¹⁹ T. Kato, Comm. Pure Appl. Math. **10**, 151 (1957).
 - ²⁰ G. Rajagopal, R. J. Needs, S. Kenny, W. M. C. Foulkes, and A. James, Phys. Rev. Lett. **73**, 1959 (1994).
 - ²¹ C. J. Umrigar, K. G. Wilson, and J. W. Wilkins, Phys. Rev. Lett. **60**, 1719 (1988).
 - ²² C. Greef and W. Lester, J. Chem. Phys. **106**, 6412 (1997).
 - ²³ A. Luchow and J. Anderson, J. Chem. Phys. **105**, 7573 (1996).
 - ²⁴ H. Eckstein, W. Schattke, M. Reigrotzki, and R. Redmer,

- Phys. Rev. B **54**, 5512 (1996).
- ²⁵ C.-J. Huang, C. Umrigar, and M. Nightingale, J. Chem. Phys. **107**, 3007 (1997).
- ²⁶ C. Filippi and C. Umrigar, J. Chem. Phys. **105**, 213 (1996).
- ²⁷ A. Szabo and N. Ostlund, *Modern Quantum Chemistry* (McGraw-Hill, New York, 1989).
- ²⁸ R. McWeeny, *Methods of Molecular Quantum Mechanics* (Academic Press, London, 1989).
- ²⁹ P. O. Löwdin, J. Chem. Phys. **61**, 55 (1957).
- ³⁰ W. Meyer, J. Chem. Phys. **58**, 1017 (1973).
- ³¹ P. H. Acioli and D. Ceperley, J. Chem. Phys. **100**, 8169 (1994).
- ³² X. P. Li, D. Ceperley, and R. M. Martin, Phys. Rev. B **44**, 10929 (1991).
- ³³ P. Löwdin, Phys. Rev. **97**, 1474 (1955); *ibid.* 1490; *ibid.* 1509.
- ³⁴ J.F. Cornwell, *Group Theory in Physics Vol. 1* (Academic Press, London, 1984), p. 81.
- ³⁵ R. Q. Hood, M. Y. Chou, A. J. Williamson, G. Rajagopal, R. J. Needs, and W. M. C. Foulkes, Phys. Rev. Lett. **78**, 3350 (1997).
- ³⁶ C. Pisani, V.R. Saunders, C. Roetti, M. Causà, N.M. Harrison, R. Orlando, and E. Aprà, *CRYSTAL 95 User Manual*, Università di Torino and CCLRC Daresbury Laboratory (1995).
- ³⁷ R. P. Feynman, Phys. Rev. **94**, 262 (1954).
- ³⁸ R. C. Morrison, J. Chem. Phys. **96**, 3718 (1992).
- ³⁹ O. W. Day, D. W. Smith, and R. C. Morrison, J. Chem. Phys. **62**, 115 (1975).
- ⁴⁰ L. Adamowicz, J. C. Ellenbogen, and E. A. McCullough, Int. J. Quantum Chem **30**, 617 (1986).
- ⁴¹ O. W. Day and D. W. Smith, J. Chem. Phys. **62**, 113 (1975).
- ⁴² W. von der Linden and P. Horsch, quoted in W. Bormann and P. Fulde, Phys. Rev. B **35**, 9569 (1987).
- ⁴³ J. R. Chelikowsky and M. L. Cohen, Phys. Rev. B **14**, 556 (1976).
- ⁴⁴ M. Rohlfing, P. Krüger, and J. Pollmann, Phys. Rev. B **48**, 17791 (1993).

FIG. 1. Occupation numbers (diagonal elements of the density matrix in the basis of LDA orbitals) plotted against the LDA energy for each \mathbf{k} -point. These are the Γ -point(\circ), Δ (\diamond), Σ (∇), and Λ (\square), points on the Δ , Σ , and Λ axes respectively. The statistical error bars are approximately equal to the sizes of the symbols for the conduction band states and are about 5 times smaller than the symbols for the valence band states.



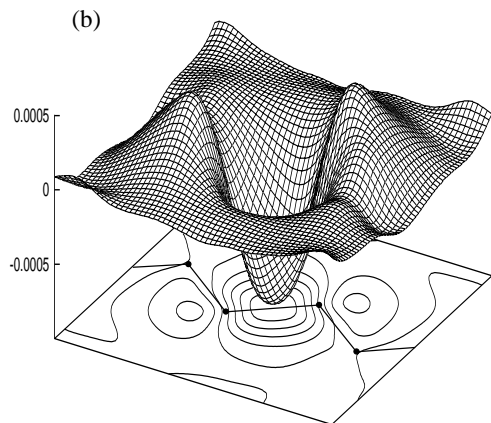
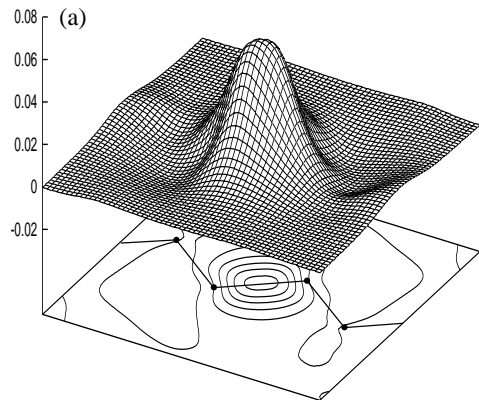


FIG. 2. (a) The VMC one-body density matrix, $\rho_{\text{VMC}}(\mathbf{r}, \mathbf{r}')$ and (b) $\rho_{\text{VMC}}(\mathbf{r}, \mathbf{r}') - \rho_{\text{LDA}}(\mathbf{r}, \mathbf{r}')$, in the (110) plane passing through the atoms with \mathbf{r} fixed at the bond center. ρ is normalized such that $\rho(\mathbf{r}, \mathbf{r}) = n(\mathbf{r})$, the charge density at the bond center. The silicon atoms and bonds are shown schematically.

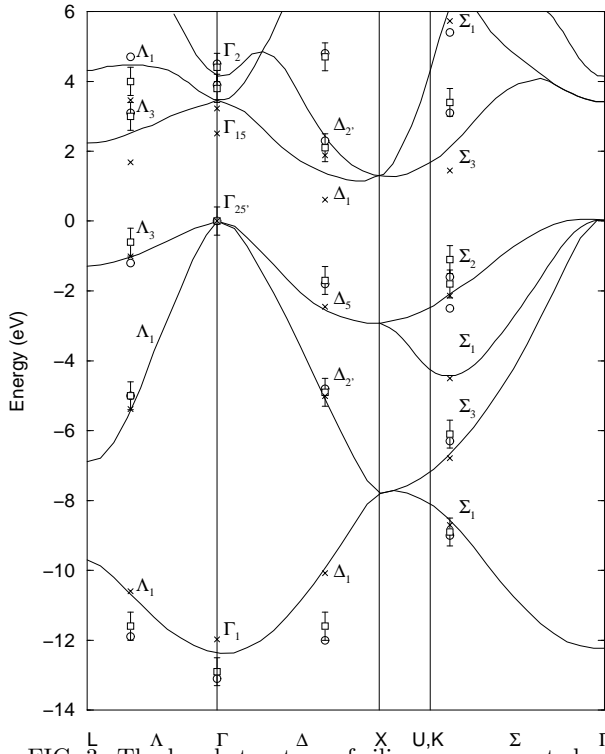


FIG. 3. The band structure of silicon, as computed within the VMC Extended Koopmans' Theorem using the cutoff interaction (\square) and the Ewald interaction (\circ), and within the LDA (\times). The results for the cutoff interaction are shown with statistical error bars. The statistical error bars for the Ewald results have been omitted for clarity, but they are the same size as for the cutoff interaction. As a guide to the eye, the empirical pseudopotential data of [43] is shown (solid lines), which is in good agreement with the available experimental data.

Band	VMC				DMC ^e	HF ^f	LDA ^g	GW ^h	Emp ⁱ	Exp ^j
	EKT ^a	EKT ^b	DEKT ^c	DEKT ^d						
$\Gamma_{2'}$	4.4	4.5	5.1	5.2	4.6	9.0	3.22	3.89	4.1	4.23,4.1
Γ_{15}	3.8	3.9	4.4	4.4	3.7	8.0	2.51	3.36	3.4	3.40,3.05
$\Gamma_{25'}$	0.0	0.0	0.0	0.0	0.0	0.0	0.00	0.00	0.0	0.00
Γ_1	-12.9	-13.1	-13.3	-13.4	-13.6	-18.9	-11.98	-11.95	-12.36	-12.5±0.6
Λ_3	4.0	4.7	5.4	5.7		9.0	3.46		4.5	
Λ_1	3.0	3.1	3.6	3.6		6.8	1.68		2.5	
Λ_3	-0.6	-1.2	-1.3	-1.5		-1.7	-1.01		-0.9	
Λ_1	-5.0	-5.0	-5.4	-5.4		-6.3	-5.38		-5.2	
Λ_1	-11.6	-11.9	-12.3	-12.5		-16.4	-10.60		-10.6	
$\Delta_{2'}$	4.7	4.8	5.7	6.0		7.2	1.88		2.4	
Δ_1	2.1	2.3	2.7	3.0		5.5	0.61		1.3	
Δ_5	-1.7	-1.8	-2.4	-2.5		-3.8	-2.45		-2.5	
$\Delta_{2'}$	-4.9	-4.8	-5.5	-5.7		-7.8	-5.01		-5.0	
Δ_1	-11.6	-12.0	-11.7	-12.2		-16.0	-10.08		-10.2	
Σ_1	6.4	5.4	6.7	6.1			5.73		6.0	
Σ_3	3.4	3.1	4.1	4.0			1.45		2.0	
Σ_2	-1.1	-1.6	-1.2	-2.0			-2.14		-2.1	
Σ_1	-1.8	-2.5	-1.9	-2.5			-4.50		-4.6	
Σ_3	-6.1	-6.3	-6.4	-6.8			-6.79		-6.7	
Σ_1	-8.9	-9.0	-9.5	-9.8			-8.70		-8.7	

TABLE I. Band energies of silicon in eV. a,b- VMC-EKT energies using the cutoff and Ewald interactions, respectively. The statistical error bars are ± 0.4 eV. c,d- Diagonal approximation to the VMC-EKT energies using the cutoff and Ewald interactions, respectively. The statistical error bars are ± 0.2 eV. e- Direct DMC calculations, with statistical error bars of ± 0.2 eV, from Ref. 9. f- Ref. 42. g- This work. h- Ref. 44. i- Ref. 43 j- From the compilation given in Ref. 44.